Bulletin of the New Zealand Society for Earthquake Engineering, Vol. 56, No. 4, December 2023

SEISMIC FRAGILITY OF REINFORCED CONCRETE BUILDINGS WITH HOLLOW-CORE FLOORING SYSTEMS

Tom C Francis[1], Eyitayo A Opabola[2], Timothy J Sullivan[3], Kenneth J Elwood[4], and Cameron J Belliss[5]

(Submitted *February 2023*; Reviewed *February 2023*; Accepted *July 2023*)

ABSTRACT

Hollow-core flooring systems were damaged in Wellington buildings during the 2016 Kaikoura earthquake (7.8 M_w) and have been shown to be susceptible to undesirable failure mechanisms (loss of seating, negative moment, and positive moment failure modes) at low drift demands. These undesirable damage mechanisms have also been observed in sub-assembly and super-assembly laboratory testing of hollow-core flooring systems and the test data obtained has enhanced the state-of-the-art knowledge of the probable seismic behaviour of hollow-core floor units. In this study, using currently available sub-assembly test data, fragility functions are defined for hollow-core flooring systems. Furthermore, the proposed fragility functions are combined with fragility information derived from nonlinear dynamic analyses for two eight-storey bare-frame reinforced concrete (RC) buildings designed based on New Zealand standards. This study shows that, in comparison with RC buildings with flooring systems that are not susceptible to gravity load failures, RC buildings with vulnerable hollow-core floors have a significantly higher likelihood of exceeding the collapse prevention limit state, as defined in this study.

https://doi.org/10.5459/bnzsee.1634

INTRODUCTION

The 2016 Kaikoura earthquake (M_w 7.8) underlined deficiencies in the seismic performance of precast flooring systems in reinforced concrete (RC) buildings in New Zealand [1]. In particular, hollow-core flooring systems, which are vulnerable to three possible failure modes - positive moment failure (PMF), loss of seating (LoS) and negative moment failure (NMF), performed poorly (Figure 1). In the Wellington region, the Kaikoura event caused moderate to high levels of ground motion intensity, particularly at 1-2 second vibration periods, which resulted in many multi-storey office buildings being subjected to damaging ground motions [2]. The observed damage to precast floors has driven a need for research into the seismic fragility of building typologies containing precast concrete flooring systems.

In the nonlinear dynamic analysis of a concrete structure, it is typically assumed that the flooring system provides a rigid diaphragm for transfer of in-plane loading and displacement restraint between the lateral load resisting elements; hence, only the primary lateral load resisting system, such as RC moment frames, are typically analysed. However, recent events have shown that inelastic deformations such as beam elongation may need to be considered, especially in the case of ductile concrete frames, which are expected to undergo large inelastic cyclic deformations. Similarly, for these types of buildings, cyclic deformation may cause damage to precast flooring systems to the point where loss of a reliable gravity load path is reached. Seismic assessment guidelines in New Zealand [3] provide procedures to estimate the building drift demand when a reliable load path for a precast flooring system is compromised.

FEMA P695 [4] proposes a simple method for consideration of non-simulated collapse modes such as collapse of precast flooring units. These non-simulated failure modes are considered simply by carrying out nonlinear response history analyses (NLRHA) and stopping the analysis at the point where the median collapse intensity of the non-simulated component is exceeded. The median collapse intensity of the component should be established based on test data and represented by an appropriate parameter, e.g., the interstorey drift demand of the superstructure corresponding to probable drift capacity of the component. Although the simplicity is beneficial, the FEMA approach does not take variability in component performance into account and failure of one of the components may not necessarily trigger overall collapse of the system. The latter issue is of particular concern if there are multiple components to be considered such as is the case with precast flooring elements. Due to these reasons, the prediction of collapse based on the failure of a single component can be overly conservative [4].

This paper aims to directly compare the fragility of reinforced concrete buildings with and without precast floors. This work considers hollow-core precast flooring units and two eight-storey case study RC frame buildings, which are designed for the Christchurch and Wellington regions. The main objective of this research is to identify the influence of precast floors on the seismic fragility of RC buildings at or near a state of collapse. However, recognising the inherent uncertainty in collapse prediction, the focus is placed on the relative fragility between structures with and without precast floors, as opposed to quantification of the exact collapse fragility.

METHODOLOGY

Case Study Building Design

The case study buildings consist of two eight-storey reinforced concrete frames designed to NZS3101 [5] using the force-based approach outlined in NZS1170.5 [6]. Two ductile frames are designed for NZS1170.5 [6] Z-factors of Z=0.30 and Z=0.39, that could be considered representative of buildings in Christchurch and Wellington, respectively.

[1] *Postdoctoral Fellow, University of Canterbury, Christchurch, tom.francis@canterbury.ac.nz*
[2] *Senior Research Fellow, University College London, United Kingdom, e.opabola@ucl.ac.uk*
[3] *Professor, University of Canterbury, Christchurch, timothy.sullivan@canterbury.ac.nz*
[4] *Chief Engineer, Ministry of Business, Innovation and Employment, Wellington, kenneth.elwood@mbie.govt.nz*
[5] *Pre-Construction Engineer, Naylor Love, Christchurch, cameron.belliss@naylorlove.co.nz*

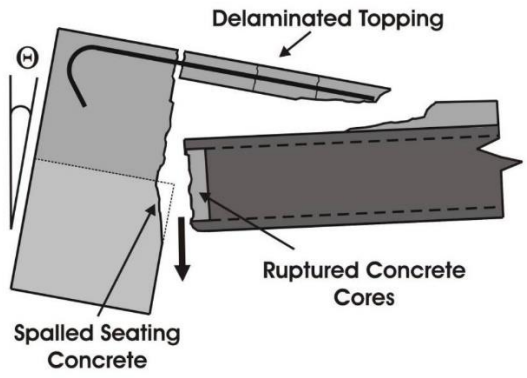

(a) Loss of seating (Jensen et al. [7])

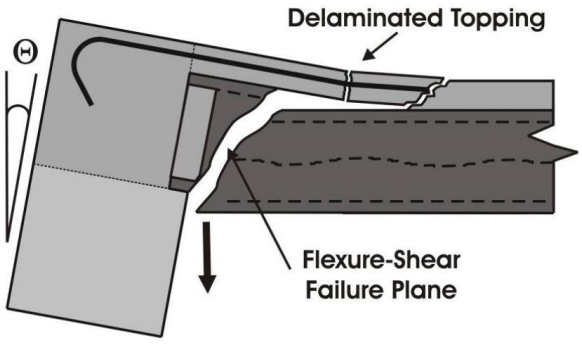

(b) Positive moment failure (Jensen et al. [7])

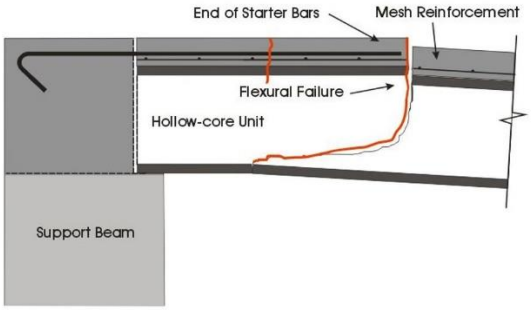

(c) Negative moment failure (Woods et al. [8])

Figure 1: The three possible failure modes of hollow-core flooring systems.

Older versions of the design standard had a Z factor of Z=0.22 for Christchurch and thus the design solution developed could be slightly conservative, as may occur in practice. The external bay widths (and corresponding hollow-core span) are 8 m for both buildings with an internal bay width of six metres. This external bay span is made to align with the fact that the typical span for 200 mm hollow-core units is 8 m, which has led to a dominance of eight metre spans for this flooring system in New Zealand urban areas. The seating details for the hollow-core units considered in this study are discussed in Hollow-Core Floor Unit Fragility Functions.

As shown in ***Figure 2***, the building has a square floor plan with lateral loads resisted by perimeter moment-resisting frames in each direction. Columns are set back from the corners of the floor plate such that no bi-directional interaction is considered in the design and assessment of the end columns. As the frame analysis is two-dimensional, a single external frame in ***Figure 2*** is considered. For both case study buildings, a frame has been designed to represent one of the East-West perimeter frames, which is required to accommodate both seismic and gravity loads. The vertical gravity load resisting frame system (i.e., internal frames) has been assumed to have sufficient strength and deformation capacity such that failure does not occur prior to the failure of the lateral-load resisting system.

Nonlinear Time History Analysis Modelling

General

The RC case study frames have been modelled numerically as two dimensional frames using the lumped plasticity modelling software Ruaumoko3D [9]. The frames are modelled with fully fixed bases, rigid diaphragms in-plane at each floor level, one component Giberson beam members and reinforced concrete (Type 1) beam-column members. Refer to Carr [10] for further details on these member types. The following section outlines the other salient features and assumptions used in the modelling of the frames.

Material Properties

For the purpose of assessment of the case study frames, the material properties used should reflect the expected strengths, not the lower bound characteristic values used in design. For steel and concrete, the yield strength and compressive strength respectively are increased as per the simple expressions in Equations (1) and (2) from Priestley et al. [11]. The stress strain relationships used in the moment curvature analysis of the sections is taken to be the default settings within Cumbia [12].

$$f_{ye} = 1.1 f_y \quad (1)$$

$$f'_{ce} = 1.3 f'_c \quad (2)$$

where f_y is the yield strength of reinforcing steel and f_c' is the concrete compressive strength. The resulting material properties assumed for design of the case-study buildings are outlined in Table 1

Table 1: Design material properties.

Symbol	f_c'	E_c	$f_{y,beam}$	$f_{y,col}$	$f_{y,trans}$
Value [MPa]	30	25000	300	500	500

Gravity Loads

Gravity loads are applied to the structure as point loads at the beam-column joints at each floor level, with no uniformly

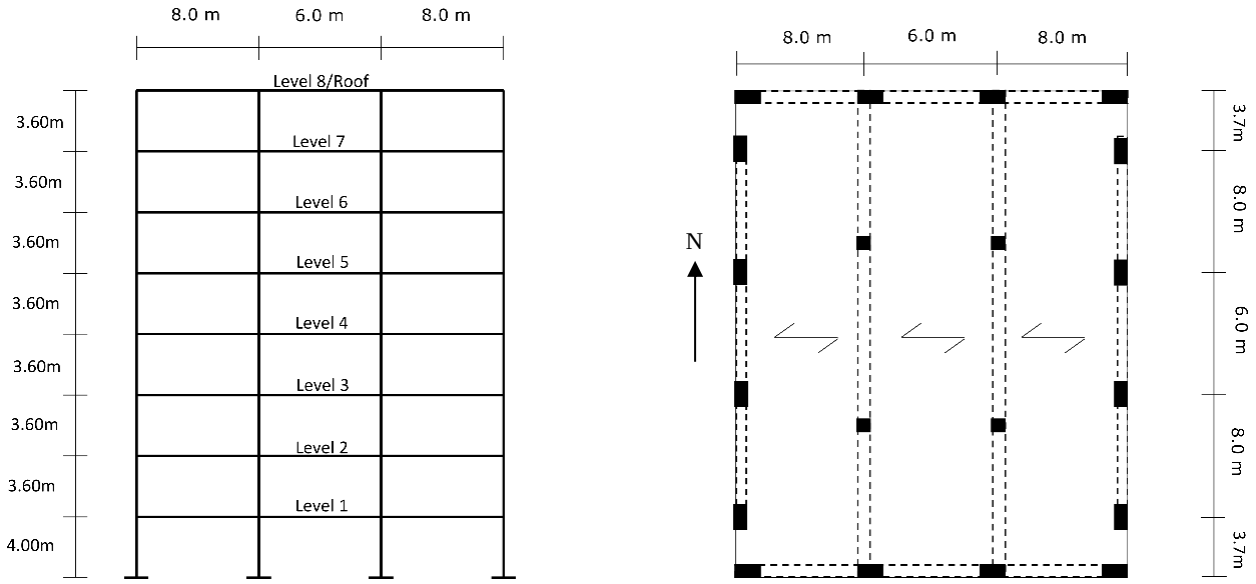

Figure 2: Frame elevation (left) and building plan (right) views of the eight-storey case study RC frame building.

distributed loading applied to the beams. The effects of not including distributed gravity loads on the beams are considered to be negligible on the inelastic member rotations obtained from NLRHA for beams with reversing plastic hinges, as shown by Pinto [13]. The magnitude of the gravity loads is the same as that used in the design of the frames for ultimate limit state seismic actions as defined by NZS1170.0 [14], being the self-weight of the structure plus 30% of the live load.

Beam-Column Joints

Following the beam-column joint modelling approach recommended in Elwood et al. [15] and ASCE 41-17 [16] for beam-column joints with $\sum M_c/\sum M_b > 1.2$, to allow for flexibility of beam-column joints, the beam elements do not have any rigid offsets, and instead run continuous between nodes. In the absence of transverse loads along the beams, the yield moments at the beam ends, now located at the centre of the beam-column joint, are adjusted such that the desired yield moment is achieved at the column face with a shear force associated with yielding at either end of the beam. Rigid offsets to the columns are maintained, being equal to half of the beam depth at the end of each column. This is required in order to allow for modelling of the axial load-moment interaction at the potential plastic hinges of the columns.

Damping

The damping model used in the analysis is a variation of the traditional Rayleigh damping model, whereby the secant damping matrix is formed using the tangent stiffness matrix of the numerical model (ICTYPE=6 in Ruaumoko3D [10]). This choice of damping model is given as a recommendation in the manual for Ruaumoko3D [10] for reducing the effects of increased damping forces with period elongation. A damping ratio of 5% is specified at the first two modes of vibration.

Moment-Curvature Response

The plastic hinges of the frames have been modelled using a modified Takeda hysteresis rule with ductility-based, between cycle strength degradation [17]. As per recommendations from Dwairi et al.[18], beams are modelled with a Takeda 'Fat' relationship, $\alpha = 0$ and $\beta = 0.6$, while columns are modelled with Takeda 'Thin' relationship, $\alpha = 0.5$ and $\beta = 0.0$. A reloading stiffness power factor of 1.0 is assumed, and the Emori unloading approach. For further details on the hysteresis model refer to Carr [10].

Figure 3 illustrates the form of the backbone curve to the hysteretic response that was implemented in the numerical model. The key parameters that must be determined to define this curve are the sections initial stiffness, K_i, yield moment, M_y, post-yield hardening ratio, r (i.e. the ratio of the post-yield stiffness to the initial stiffness), the pre-capping plastic curvature capacity, $\phi_{cap,pl}$, post-capping plastic curvature capacity, ϕ_{pc}, and the residual moment capacity, M_r. The plastic hinge length (l_p), sectional initial stiffness, yield moment, and post-yield hardening ratio have been defined by the bilinear approximation to the moment curvature relationship obtained from section analysis in Cumbia [12] with gravity only axial loads. In the cases where the post-yield hardening ratio obtained from Cumbia was zero or negative, it was increased and set to a minimum value of 0.001.

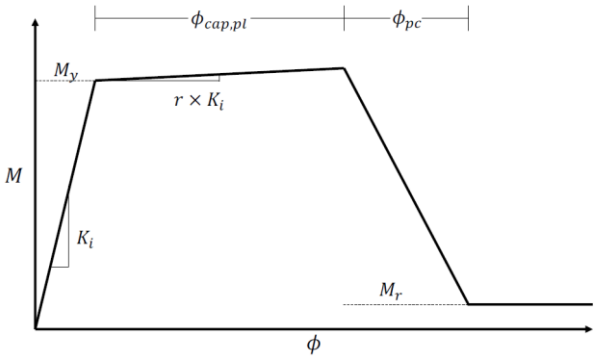

Figure 3: Illustration of parameters of strength degrading hysteretic backbone curve implemented in Ruaumoko3D [9].

The plastic curvature capacity to the peak capping point, $\phi_{cap,pl}$, was defined using a simplified empirical equation, proposed by Haselton and Deierlein [19]:

$$\phi_{cap,pl} = \frac{1}{l_p} 0.13(1 + 0.55 a_{sl})(0.13)^{\nu}(0.02 + 40\rho_s)^{0.65}(0.57)^{0.01 f_c'} \quad (3)$$

The form of the equation is similar to that given by Fardis [20] for predicting the ultimate chord rotation capacity of beam-columns. However, this equation is used to predict the plastic chord rotation capacity of the member between yielding and achieving peak strength, not the ultimate rotation capacity. This calculated rotation capacity is a function of the axial load ratio, v, transverse reinforcement ratio, ρ_s, and the lower bound characteristic concrete compressive strength f_c', with $a_{sl} = 1$ where bond slip can occur, and 0 otherwise (and in this study it was assumed that bond slip would not occur).

The simplified expression for the post-capping plastic curvature capacity, ϕ_{pc}, is obtained from a similar equation proposed by Haselton and Deierlein [19], given in Equation (4), as a function of the same parameters, but limited to a maximum rotation of 0.1 radians.

$$\phi_{pc} = \frac{1}{l_p} 0.76(0.031)^{v}(0.02 + 40\rho_s)^{1.02} \leq \frac{0.10}{l_p} \qquad (4)$$

Finally, the residual strength of the member is set to 1% of the yield strength. This factor, while uncertain, is not considered by previous researchers [21] to have significant affect the outcome of the analyses.

P-Δ Effects

Second order *P*-Δ effects are taken into account using 'Large Displacement' analysis in Ruaumoko3D. To account for the contribution to *P*-Δ effects from gravity loads within the seismic tributary area, that do not vertically load the frame, a *P*-Δ gravity column is included in the model, modelled as a truss element between floors, with lateral displacements constrained by the floors. This is done to introduce the total vertical gravity loads but provide no additional lateral resistance to the building.

Ground Motion Selection

Ground motions to be used in NLRHA's were scaled using probabilistic seismic hazard analysis (PSHA) together with the generalised conditional intensity measure (GCIM) approach [22]. PSHA was performed for Wellington for V_{s30} = 450 ms^{-1} and Christchurch for V_{s30} = 250 ms^{-1} on OpenSHA using New Zealand-specific rupture forecast models and attenuation relationships for the selected intensity measure (IM) of spectral acceleration at two seconds [23]. The ground motion selection does not account for basin edge effects and as such, the case-study buildings are assumed to be located where basin effects are minimal. Ground motion records across nine hazard levels, each containing 20 orthogonal records, were adopted in this study. The resulting seismic hazard curves for the Christchurch and Wellington sites are shown in Figure 4. Refer to Yeow et al. [23] for further details on the ground motion selection approach. The nine intensity levels for both locations refer to annual exceedance rates from 80% in 50 years up to 0.2% in 50 years. Note that this research was completed prior to the release of the 2022 National Seismic Hazard Model. The conditioning period of two seconds was chosen to align with the first mode periods of the Christchurch and Wellington models of 2.22 s and 2.02 s respectively.

Definition of Individual Building and Precast Floor Fragility Functions

Previous studies on collapse fragility [24-26] have typically only considered the performance of the seismic force resisting system. This study aims to also consider the uncertainty in the performance of the hollow-core precast floors when assessing the fragility of the building as a whole. Hence, fragility functions are required for both: (a) the case study buildings without precast flooring (i.e. the bare-frames) and (b) the hollow-core flooring units.

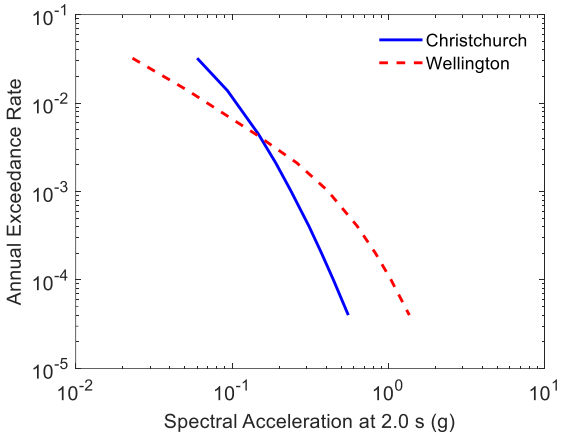

Figure 4: Probabilistic seismic hazard curves for spectral acceleration at two seconds for (a) Christchurch and (b) Wellington from Yeow et al. [23].

Bare-Frame Fragility Functions

The building fragility functions are defined as the probability of exceeding the collapse-prevention limit (CPL) of the building which is assumed to occur at an interstorey drift of 5%. The CPL is justified in its use as a limit state due to the uncertainty and loss of confidence in the performance and modelling of the plastic hinge regions of the beams past this drift demand [27]. There is uncertainty in the value of drift to be used for this limit state and one could expect that the exact value will depend on the aspect ratio of beams, the material properties and the reinforcement detailing adopted in the plastic hinge regions (see, for example, Priestley et al. [11]). This limit state is analogous to a limit state with significant structural damage, including bar fracture at multiple hinges thus limiting repair options, although some margin against collapse may still be anticipated. The approach adopted here reflects the higher confidence in the validity of modelling results up to CPL compared to modelling all the way to collapse of the structure. It is noted that the 5% drift at CPL is significantly higher than the drifts expected of the case study frame buildings for ground motion intensities at the ultimate limit state (500-year return period).

Fragility functions for the CPL of the RC frame buildings are determined using the multiple-stripe analysis approach [28] with ground motions conditioned to a period of two seconds. The conditioning period is similar to the fundamental period of the buildings which allows for an easily quantified increase in spectral demand with increasing intensity levels, minimising the effect of record-to-record variability. Lognormal fragility functions are fitted to the multiple-stripe data using maximum likelihood estimation based on the recommendations of Baker [29]. The building fragility functions can be defined using Equation 5:

$$P[CPL_{frame}|IM] = \Phi\left(\frac{\ln(IM/\theta)}{\beta}\right) \qquad (5)$$

where $P[CPL_{frame}|IM = im]$ is the probability of exceeding the CPL given an intensity measure IM, Φ is the standard normal cumulative distribution function, θ is the median IM of the fragility function and β is the standard deviation of $\ln(IM)$.

Hollow-Core Floor Unit Fragility Functions

To assess the overall fragility of buildings with hollow-core floors, fragility functions for the hollow-core flooring units in terms of interstorey drift are required. Hollow-core floor units are susceptible to three different failure modes, loss of seating

(LoS), positive moment failure (PMF), and negative moment failure (NMF), each affecting the gravity load capacity. Three different fragility functions are determined, one for each failure mode. The floor fragility functions are defined as the probability of exceeding the Collapse Prevention Limit (CPL) given an Interstorey Drift Ratio (IDR).

$$P[CPL_{floor}|IDR] = \Phi\left(\frac{\ln(IDR/\theta)}{\beta}\right) \quad (6)$$

Similar to selection of the CPL for the bare-frame assessment described above, the CPL for hollow-core floors is intended to represent a state of damage which significantly impacts the reliability of structural engineering models to predict the performance and damage which is likely to limit repair options. For this study the CPL for a hollow-core floor unit is taken as the drift at which "loss of reliable load path" is reached, a limit determined based on laboratory tests. A series of 'super-assembly' and 'sub-assembly' tests have been carried out by various researchers [30-32] for hollow-core floor support connections found in New Zealand buildings. Corney et al. [33] provides a detailed description of these test programmes and defines three possible failure modes for hollow-core floor units observed in the tests: LoS, PMF, and NMF. Each of these failure modes impacts the gravity load carrying capacity and has the potential to result in collapse of the unit. However, the exact drift at collapse of the floor unit is nearly impossible to predict due to variability in boundary conditions, impact of vertical accelerations, variability of tension capacity of concrete, load sharing between units, etc. The tests do, however, provide critical data as to when the floor unit may begin to drop relative to the supporting beam. Corney et al. [33] assumes that once the floor unit drops more than 2mm relative to the supporting beam, there is a "loss of reliable load path" for transfer of gravity loads from the floor unit to the supporting beam. At this point it is assumed the CPL has been exceeded for the hollow-core unit.

Table 2 shows the drift capacities of hollow-core unit tests reported by Corney et al. [33] for the three considered failure modes.

Table 2: Interstorey drift at CPL from Corney et al. [33] for three hollow-core unit failure modes: LoS, PMF and NMF.

	Interstorey drift at exceedance of limit state [%]		
Test number	**LoS**	**PMF**	**NMF**
1	1.71	1.0	1.0
2	1.71	1.76	1.1
3	2.5	3.0	3.8
4	2.0	-	1.88
5	2.0	-	-

The NZ Guidelines [3] provide provisions for seismic assessment of hollow-core floors in Appendix C5E. The seismic assessment procedure entails evaluating the probable drift capacities of hollow-core floors associated with the three failure modes. The dominating failure mode corresponds to that with the lowest computed probable drift capacity, which is subsequently compared with an estimate of the drift demand to assess if the floor has exceeded the CPL. (Note the terminology of CPL is not used in the NZ Guidelines [3] but used here for analogy with the CPL for the building frame described previously.)

According to Appendix C5E of the NZ Guidelines [3], the drift capacity corresponding to LoS for a hollow-core floor unit is dependent on beam elongation, rotation of the supporting beam, and spalling of the hollow-core unit and supporting ledge. Puranam et al. [34] provided a comparison of the measured drift capacities from sub-assembly tests with those predicted using the provisions of NZ Guidelines [3] (see Figure 5). For the five LoS-critical test specimens, the NZ Guidelines procedure provides an estimate with a mean ratio of measured to calculated drift capacity of 1.1 and dispersion, β, of 0.18. Based on field evidence, the provided in-situ seating for a precast floor unit will frequently be less than the specified seating. To account for uncertainty in seating length, the NZ Guidelines requires the specified seating to be reduced by a 20 mm construction tolerance (unless the in-situ seating is directly measured). Here it is assumed 20 mm represents a confidence interval of one standard deviation, $\pm 1\sigma$, in the variation of in-situ seating; hence, a mean seating length assumed to be equal to the specified value of 50 mm corresponds to a β equal to 20/50=0.4. Using the SRSS approach, the combined dispersion for the drift capacity of a LoS-critical hollow-core unit is taken as 0.45.

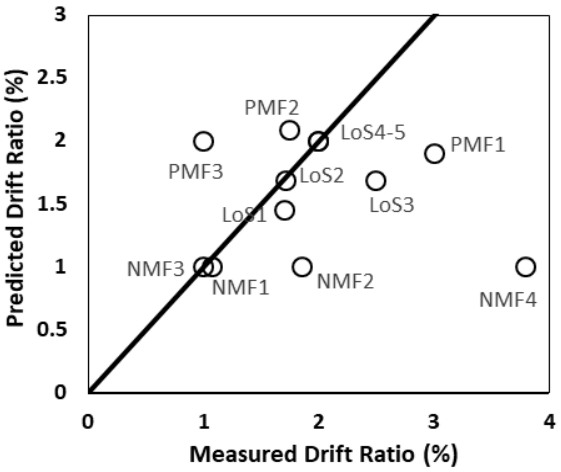

Figure 5: Relationship between measured drift capacities of test units, exhibiting the three failure modes, to those predicted using the provisions of NZ Guidelines [3] (Adopted from Puranam et al. [34]).

The development of PMF in a hollow-core unit is dependent on cracking strength of the hollow-core unit, bond and development of prestressing strands, and coefficient of friction between the hollow-core unit and the support ledge. According to the NZ Guidelines [3], the drift capacity of a PMF-critical hollow-core unit corresponds to the drift at which the computed probable support deformation from beam elongation and rotation exceeds the diameter of the prestressing strands in the unit (typically 12.5 mm). Figure 5 presents a comparison of the measured drift capacities of PMF-critical units to those predicted using the provisions of NZ Guidelines [3]. For the three PMF-critical test specimens, the NZ Guidelines procedure provides an estimate with a mean measured to calculated ratio of 0.97 and dispersion, β, of 0.52. Note that the NZ Guidelines assume this failure mode is precluded by seating the unit on a low-friction bearing strip as is required for buildings in New Zealand since 2006.

The development of a NMF at the support of a hollow-core unit is associated with deformation compatibility as the supporting beam rotates away from the hollow-core unit. Hollow-core floors constructed with short and strong starter bars and low gravity loads are more susceptible to NMF at the termination of the starter bars [34]. Due to the challenge of accurately calculating the drift at which NMF leads to a vertical dislocation of the floor unit, a drift capacity of 1% is used by NZ Guidelines [3] for NMF-critical hollow-core floor units as a conservative limit based on the limited available test data (see Table 2). A NMF-critical unit is one in which the negative moment demand at the end of the starter bars exceeds the

negative moment capacity. For the four NMF-critical test specimens, the NZ Guidelines procedure provides an estimate with a mean ratio of 1.95 and dispersion, β, of 0.6.

To develop the fragility functions for the hollow-core floor units in the adopted archetype buildings, the drift capacities for the three failure modes were computed in accordance with the provisions of Appendix C5E of the NZ Guidelines [3]. For LoS and PMF modes, the computed drift capacities were taken as the median values, while the 1% limit for NMF mode was considered to represent the 25th percentile value. The selection of the 25th percentile value was simply based on judgement, as a more refined assessment of this value was not considered advisable given the limited data available. Furthermore, the β values noted above, based on the available experimental data, were adopted to quantify the uncertainty associated with predicting the probable drift capacity of the hollow-core units. Further testing of hollow-core floor units would enable improved estimates of the fragility curves for each of the failure modes. The estimated fragility curves for all three failure modes, using the provisions of Appendix C5E of the NZ Guidelines [3] for the case study buildings with 200mm units, are shown in Figure 6.

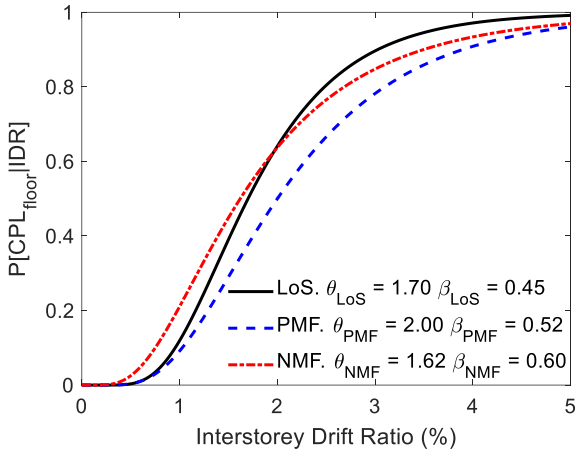

Figure 6: Hollow-core floor fragility functions and lognormal fragility curve parameters derived from test data for the three considered failure modes: LoS, PMF and NMF.

It should be noted that the median interstorey drift at exceedance of the considered damage state for all three modes is below the 2.5% drift limit imposed by NZS1170.5 [6], highlighting the issues with these types of floors under strong shaking intensities and justifying the need for understanding the effect on the overall building fragility.

The fragilities described above do not consider web cracking due to torsion or incompatible displacements. According to the NZ Guidelines [3] assessment procedure, such web cracking will potentially reduce the PMF drift capacity, thereby reducing the PMF fragility in Figure 5 and considered in this study. However, the vulnerability of a unit to web cracking is highly dependent on the exact location of the unit in the building and the specific boundary conditions. In this study we seek to identify the change in fragility considering only generic support conditions for hollow-core units, without the details required to identify if a unit is vulnerable to web cracking. Hence, web cracking is ignored in the current study and the resulting fragilities for PMF should be considered an upper bound for real buildings.

Combining Floor and Building Fragility Curves

A combined fragility curve for the building and floor system can be determined using the well-known probability relationship

$$P[A \cup B] = P[\mathrm{A}] + P[\mathrm{B}] - P[A \cap B] \tag{7}$$

where $P[A]$ and $P[B]$ are the respective probabilities of event A and B occurring and $P[A \cap B]$ is the intersection of probabilities of the events A and B occurring. $P[A]$ and $P[B]$ are subsequently used to define the fragility functions for the bare-frame and flooring systems respectively as defined by Equation 5 and 6. Events A and B are considered to be independent which means the failure of the flooring system does not affect the probability of failure of the bare-frame and vice-versa. This does not imply that the flooring system has no effect on the frame capacity in practice. Hollow-core units may marginally increase the global strength and stiffness which should be carefully considered in the modelling approach if the effect is likely to be significant. However, the strength addition of precast flooring units is neglected in this modelling work and the focus is on the magnitude of decreased robustness observed in buildings with unreliable precast flooring systems. Taking this independence into consideration, Equation 7 can be rewritten as

$$P[A \cup B] = P[\mathrm{A}] + P[\mathrm{B}] - P[A]\mathrm{P}[B] \tag{8}$$

Substituting notation for the floor and building fragility functions, Equation 8 can be rewritten as:

$$\begin{aligned} &P[CPL_{frame}|IM \cup CPL_{floor}|IDR] \\ &= P[CPL_{frame}|IM] + P[CPL_{floor}|IDR] \\ &- P[CPL_{frame}|IM]\, P[CPL_{floor}|IDR] \end{aligned} \tag{9}$$

Once both the individual floor and building fragility functions are determined, the combined fragility can be calculated at a given IM level using Monte Carlo simulation: For each IM level, i, the value of the building only fragility function, $P[CPL_{frame}|IM]$ from Equation 5 is determined. Then, at the same considered IM level, a value of peak interstorey drift is randomly selected from the NLRHA results. Using this drift, the value of the floor fragility function, $P\left[CPL_{floor}|IDR\right]$, is determined from Equation 6. Using Equation 9, the combined fragility is calculated. The process is repeated at the same IM level using Monte Carlo simulation for a suitable number of occurrences, n_{sim}, that results in minimal change to the value of the combined fragility (should the Monte Carlo simulation be repeated) as given in Equation 10.

$$\begin{aligned} &P\left[CPL_{frame}|IM \cup CPL_{floor}|IDR\right]_i \\ &= \frac{1}{n_{sim}} \sum_{j=1}^{n_{sim}} P[CPL_{frame}|IM \\ &\cup CPL_{floor}|IDR]_{j \ldots n_{sim}} \end{aligned} \tag{10}$$

Once the combined fragility has been calculated, the analysis moves to the next IM level until all levels have been completed. The combined fragility is now known for each IM level with the final task being to fit lognormal parameters to the data. This can be done using maximum likelihood estimation or another appropriate curve fitting method such as minimising the sum of squares error (SSE), which is the approach adopted in this paper.

RESULTS

Nonlinear Response History Analysis Results

Figure 7 shows peak interstorey drift as a function of spectral acceleration at two seconds from the NLRHAs for the Christchurch and Wellington case study buildings. Note that once the building model has reached dynamic instability, the

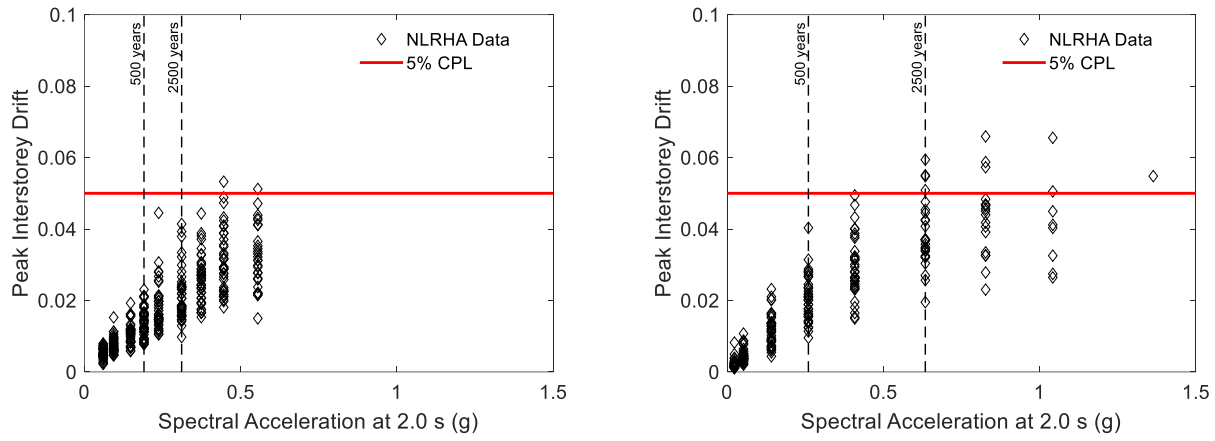

(a) CHC (b) WLG

Figure 7: Peak inter-storey drift as a function of the spectral acceleration at T = 2.0 s for the (a) CHC and (b) WLG buildings. The collapse-prevention limit (CPL) is considered at an inter-storey drift of 5%.

interstorey drifts registered by Ruaumoko3D (Carr, 2018) become very large and are not displayed in the plots. Dynamic instability generally occurs at drifts above 5%, which is the same as the assumed drift capacity at the CPL, further justifying its use as a meaningful limit state for defining fragility functions.

It is important to note that the seismicity of the Wellington region is significantly higher than for Christchurch, as is evident in a comparison of the hazard curves as shown in Figure 4. Therefore, while the Wellington building is designed for higher forces, there are significantly more records causing the model to exceed the CPL compared to Christchurch.

When dynamic instability is reached in Ruaumoko3D, the drift values reported can be very large. Therefore, the distribution of drifts for high intensity levels with records causing collapse of the structure do not follow an expected normal or lognormal distribution but are heavily skewed towards high drift values which don't make practical sense. To deal with this in the Monte Carlo simulation for determining the combined building fragility, records which reach dynamic instability are assumed to have caused a maximum drift of 10%. Looking at Figure 6, it is apparent that the value of the fragility functions for all three failure modes at this large drift is very close to one; hence, both the building and floor fragilities can be considered to have exceeded the proposed CPL.

The data in Figure 7 is used to determine CPL fragility functions for the Christchurch and Wellington buildings without precast floors using maximum likelihood estimation. To determine fragility using this method the following information is required per Baker [29]:

1. The number of records causing a certain limit state to be exceeded (i.e. the CPL of 5% considered in this paper).
2. The number of ground motions at each intensity level.
3. The values of the IM at each level.

The resulting bare-frame fragility functions for Christchurch and Wellington buildings are compared in Figure 8.

Combined Hollow-Core Floor Units and Building Fragility Functions

The fragility combination approach detailed in *Combining Floor and Building Fragility Curves* is used to determine the combined fragility functions of the buildings with precast flooring systems. The three different floor failure modes and corresponding fragility functions in Figure 6 are combined with the fragility functions for the bare-frames (Figure 7) resulting in the combined fragilities shown in Figure 9. As anticipated, the probability of exceeding the CPL is shown to increase significantly for buildings with precast flooring systems. For the Christchurch and Wellington buildings without precast floors modelled, the median intensity at the CPL is 0.60 g and 0.69 g, respectively, with corresponding dispersions of 0.21 and 0.37. It is an expected result that the Wellington model has a slightly higher capacity which is due to higher design actions for the Wellington region compared to Christchurch. Considering the LoS failure mode and assuming a specified seating of 50 mm, the median combined capacity is found to be 0.25 g and 0.22 g for the Christchurch and Wellington buildings, respectively, and significantly less than the bare-frames. Note that the Christchurch building is now shown to have a higher capacity compared to the Wellington case when the precast floors are considered. This makes sense due to the higher drifts experienced by the Wellington building when directly comparing to Christchurch based on annual exceedance rates (Figure 7) and the fact that $P[CPL_{floor}]$ is dependent on the interstorey drift demand. Similar trends are observed for the PMF and NMF failure modes (Figure 8c-f). For PMF, the medians of the IM for Christchurch and Wellington are 0.30 g and 0.26 g with dispersions of 0.52 and 0.56, respectively. For NMF the medians of the IM for Christchurch and Wellington are 0.23 g and 0.21 g with dispersions of 0.64 and 0.65, respectively.

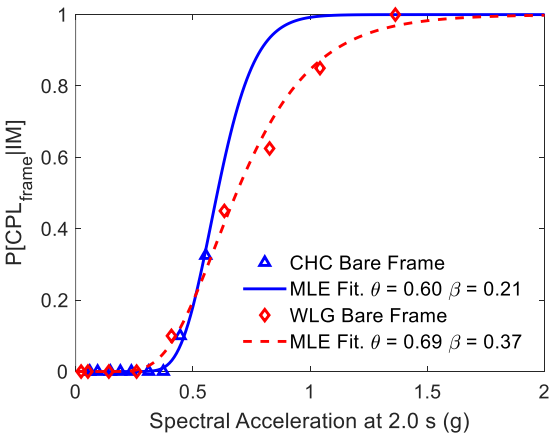

Figure 8: Comparison of the Christchurch and Wellington bare-frame fragility functions.

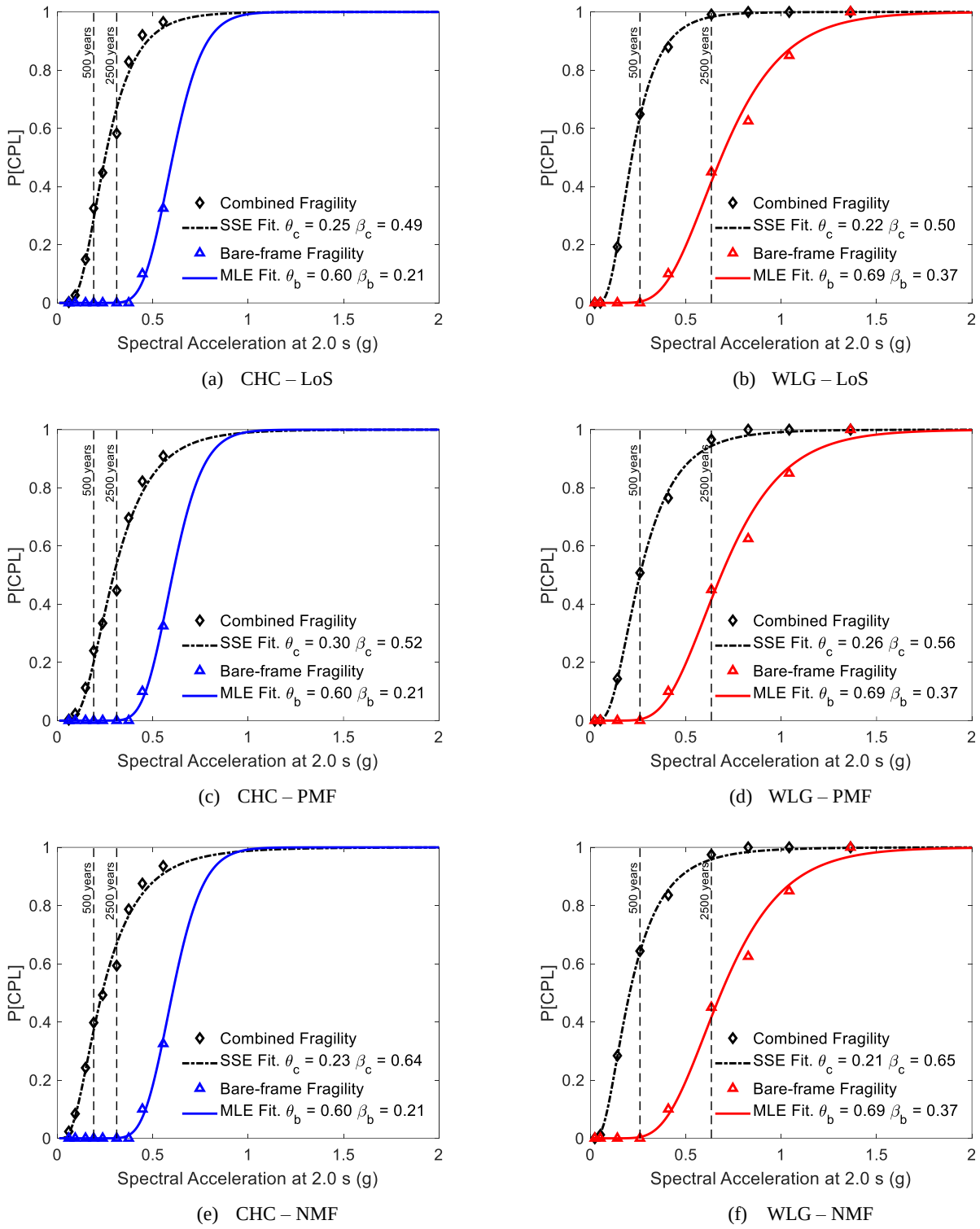

Figure 9: Comparison of the RC building fragility with the combined fragility considering global storey floor fragility for (a) CHC – LoS (b) WLG – LoS (c) CHC – PMF, (d) WLG – PMF, (e) CHC – NMF, and (f) WLG – NMF.

Analysis of the floor-only fragility functions (Figure 6) suggests that the most damaging failure mode, considering median drift at the floor CPL, is NMF followed by LoS then PMF. This result carries into the combined fragilities as expected and buildings with hollow-core floors susceptible to NMF are shown to be more vulnerable with the combined fragility functions shifting further left. LoS capacity is more reliably predicted and from results shown in Figure 8, buildings susceptible to this failure mode are shown to have slightly favourable fragilities compared to NMF. Recall that the NMF fragilities shown here are conditioned upon having units with a negative moment demand at the end of the starter bars exceeding the negative moment capacity. Puranam et al. [34] has demonstrated, using a database of Wellington buildings with hollow-core floors, that units in the majority of buildings will not be NMF-critical and thus would be governed by LoS or PMF.

Varying the parameters of the floor fragility function has a large impact on the combined fragility, particularly for values in the range of lognormal fragility parameters determined from testing. If the median of the floor fragility function is large

compared to the median of the bare-frame fragility, then there is almost no change in the combined fragility. Conceptually this makes sense, as an increase in the median collapse intensity of a non-simulated failure mode will reduce the likelihood of this mode developing. The fragility in this case, with robust floor-beam connections that are assumed to not collapse, will tend towards the bare-frame fragility functions determined without consideration of the flooring system. Büker et al. [35] showed that hollow-core floors with "strongback retrofits" were able to sustain building drifts up to 5% without loss of gravity load carrying capacity. Therefore, buildings with this type of careful retrofit would be expected to have similar fragility to the bare-frame.

Mean Annual Frequency of Exceeding the CPL

A useful metric for comparing the performance of structures is the mean annual frequency (MAF) of collapse, λ_c. For this paper the MAF of exceeding the CPL, λ_{CPL}, is used instead but represents a similar metric as the MAF of collapse. The MAF of exceeding the CPL is determined using the convolution of the hazard curves shown in Figure 4 with the relevant building fragility for the corresponding location:

$$\lambda_{CPL} = \int_{IM} P(CPL|IM = im)|d\lambda(im)| = \int_{IM} \Phi\left(\frac{\ln(im/\theta)}{\beta}\right)|d\lambda(im)| \quad (11)$$

where $P(CPL|IM = im)$ is the fragility function of the building or combined building and floor fragility functions as previously defined and $d\lambda(im)$ is the derivative of the hazard curve, $\lambda(im)$, at intensity im. Both the bare-frame building and buildings with hollow-core floors can then be independently considered and compared in terms of instances per year where the CPL is exceeded (Table 3).

The 5% drift limit for defining the CPL for both case study buildings, regardless of design location results in a higher MAF of exceeding the CPL for the bare-frame in Wellington where the drift demand is higher. Similarly, the MAF of exceeding the CPL for the buildings with hollow-core floors is higher in Wellington than Christchurch; however, the increase is not as significant as for the bare-frame. The closer agreement and the larger MAF for building with hollow-core floors reflects the fact that drifts at CPL for floors are considerably smaller than 5% and will be exceeded at lower return periods.

The ratio of λ_{CPL} for the buildings with hollow-core floors to that of a bare-frame building (i.e., $\lambda_{CPL,hollow-core}/\lambda_{CPL,bare-frame}$), indicates the relative vulnerability of a building with hollow-core floors compared to buildings with robust flooring systems. For Wellington, this ratio ranges from 6.70 to 9.08 while for Christchurch this ratio ranges from 79.7 to 166, depending on failure mode. The high ratios for Christchurch are reflective of the low MAF of collapse for the bare-frame in lower seismicity, rather than poorer performance of the floor system.

DISCUSSION

It is important to recall that the fragility functions for the failure modes considered in this study are based on the assessment methodology of Appendix C5E of the NZ Guidelines [3]. As shown in Table 2, there are limited data to validate the derived fragility functions. However, the intent of the current study is to demonstrate the increased risk with the presence of hollow-core floors (e.g. 6 to 9 times increase in MAF for the Wellington building), based on the state-of-practice assessment methodology. Additional experimental test data from sub-assembly and super-assembly laboratory testing of hollow-core flooring systems are needed to refine these fragility functions. Future analytical studies could use such refined fragility functions for improved vulnerability assessment of buildings with hollow-core floors.

As shown in Figure 6, the floor fragility function dispersions for PMF and NMF (β = 0.52 and 0.60, respectively) are significantly higher than that for LoS (β = 0.45) when considering testing data only. This indicates that PMF and NMF can be less reliably predicted using the NZ Guidelines [3] and consequently, smaller interstorey drifts still have a significant probability of causing failure. The lower dispersion for LoS could be attributed to the fact that this failure type does not depend on the complexity of crack propagation within the hollow-core unit, but occurs due to geometric considerations based on the seating length, spalling, and interstorey drift demand. These are more easily quantified than the factors influencing the point at which PMF and NMF occur (e.g. tension capacity of concrete, bond to strand, etc). This fact is evidenced by Figure 5, which compares the numerically predicted drift of the superstructure at failure with the measured results from testing. Predictions which match testing values lie on the solid line which has a slope of 1:1. It can be seen that the LoS ordinates are mainly centred around this line while PMF and NMF usually have more variance. Despite the reliability in predicting the drift capacity of hollow-core floors susceptible to LoS an increased dispersion of 0.45 is adopted for the LoS failure mode due to real life observations which indicated that the specified seating is often not provided in the field, with 20 mm discrepancies commonly noted. This dispersion was not represented in the tests by Corney et al. [33] as the seating length is known exactly in the laboratory tests.

One cause of uncertainty is the fact that the hollow-core floor tests did not consider identical configurations which results in different predicted drifts being calculated for each configuration. However, for the purposes of this research it is acceptable to have different configurations for a given failure mode as this would represent the real-life scenario where

Table 3: Comparison of the mean annual frequency of collapse for reinforced concrete buildings with and without hollow-core concrete flooring systems.

	Frame	Floor failure mode	MAF of exceeding the CPL, λ_{CPL} [exceedances/year] [x10-5]	$\lambda_{CPL,hollow-core}/\lambda_{CPL,bare-frame}$
Bare-frame	CHC	-	1.92	-
	WLG	-	44.6	-
Building with hollow-core flooring systems	CHC	LoS	223	116
		PMF	153	79.7
		NMF	319	166
	WLG	LoS	361	8.09
		PMF	299	6.70
		NMF	405	9.08

different buildings may have different construction details. Mathematically, the effect of different flooring configurations is captured by the dispersion, which has already been accounted for in this paper by using the measured drifts of multiple configurations to determine fragility functions. In addition, capturing the dispersion from different configurations allows this work to apply more generally to RC buildings with precast floors rather than a single type of building with a single hollow-core flooring configuration. This is desirable as the aim of the paper is to show the large change in fragility of buildings with unreliable flooring systems rather than exactly quantifying the fragility. In any case, generalisation of a particular fragility model for all buildings of a particular typology (i.e. RC buildings) is commonplace for performance based earthquake engineering, loss assessments, and vulnerability assessments.

CONCLUSION

This paper has compared the fragilities of RC frame buildings with and without hollow-core floors. The fragilities were developed for the "collapse-prevention limit" (CPL) defined herein as an interstorey drift of 5% on the bare-frame or the hollow-core floor units experiencing "loss of reliable load path" due to loss of seating (LoS), positive moment failure (PMF) or negative moment failure (NMF) as defined by the NZ Guidelines (2018). Exceeding these limits does not mean the frame or floors have collapsed, but rather that damage has occurred which significantly impacts the reliability of structural engineering models. It may be viewed as a lower bound on the actual point of collapse.

For floor units vulnerable to all three failure modes, NMF tends to be the most likely failure mode, followed by LoS and PMF. In addition, NMF is less reliably predicted with a dispersion of drift capacity at failure of 0.60 compared to 0.52 for PMF and 0.45 for LoS when considering the floor units by themselves. For units protected from NMF (e.g., longer starters), LoS is the most likely failure mode.

For a given shaking intensity, RC frame buildings with hollow-core flooring systems are more likely to exceed the CPL compared to the bare-frame equivalent. The median $S_a(T_1)$ at the CPL for the eight-storey bare-frame building was 0.60 g and 0.69 g for the Christchurch and Wellington buildings, respectively. Considering non-simulated failure of the hollow-core flooring system results in the median fragility for the Christchurch building reducing to 0.25 g, 0.30 g, and 0.23 g for LoS, PMF, and NMF, respectively. Likewise, the median CPL for the Wellington building reduces to 0.22 g, 0.26 g, and 0.21 g for LoS, PMF, and NMF, respectively. For the building in Wellington, the mean annual frequency of exceeding the CPL is approximately 6 to 9 times higher for a building with hollow-core floors compared to a building with a robust or retrofitted floor system not vulnerable to loss of gravity load support. These results emphasise the importance of retrofit of buildings with hollow-core floors to reduce seismic risk in New Zealand centres.

Further testing of hollow-core floor systems is encouraged to improve the fragilities proposed in this paper. Building fragilities such as those described in this paper can be used in conjunction with building inventories to assess probable city-wide losses in the case of major earthquakes. Further development of fragility curves for different building archetypes and locations would support such community-level loss studies.

ACKNOWLEDGEMENTS

This research has been partly funded through the BRANZ-funded ReCast Project via the University of Auckland, and this support is gratefully acknowledged. In addition, this project was partially funded by the Resilience to Nature's Challenges Project and Te Hiranga Rū QuakeCoRE, an Aotearoa New Zealand Tertiary Education Commission-funded Centre. This is QuakeCoRE publication number 878.

REFERENCES

1 Henry RS, Dizhur D, Elwood KJ, Hare J and Brunsdon D (2017). "Damage to concrete buildings with precast floors during the 2016 Kaikoura earthquake". *Bulletin of the New Zealand Society for Earthquake Engineering*, **50**(2): 174–186. https://doi.org/10.5459/bnzsee.50.2.174-186

2 Bradley BA, Razafindrakoto HNT and Polak V (2017). "Ground-motion observations from the 14 November 2016 Mw 7.8 Kaikoura, New Zealand, earthquake and insights from broadband simulations". *Seismological Research Letters*, 740–756. https://doi.org/10.1785/0220160225

3 MBIE. (2018). *Seismic Assessment of Existing Buildings—Section C5: Concrete Buildings*. Ministry of Business, Innovation and Employment, Wellington, NZ.

4 FEMA (2009). *FEMA P695—Quantification of Building Performance Factors*. Federal Emergency Management Agency, Washington, DC, USA

5 Standards New Zealand (2006). *NZS3101:2006—Concrete Structures Standard*. Standards New Zealand, Wellington, NZ.

6 Standards New Zealand (2004). *NZS1170.5—Part 5: Earthquake Actions—New Zealand*. Standards New Zealand, Wellington, NZ.

7 Jensen JP, Bull DK and Pampanin S (2007). "Experimental investigation of existing hollowcore seating connection seismic behaviour pre and post retrofit intervention". *NZSEE Annual Conference*, Palmerston North, NZ.

8 Woods LJ, Fenwick RC and Bull DK (2008). "Seismic performance of hollow-core flooring: The significance of negative bending moments". *NZSEE Annual Conference*, 11-13 April, Wairakei, NZ.

9 Carr A (2018). *Ruaumoko 3D - Inelastic Dynamic Analysis Software*. Carr Research Ltd.

10 Carr A (2013). *Ruaumoko Manual—Volume 3*. Carr Research Ltd.

11 Priestley MJN, Calvi GM and Kowalsky MJ (2007). *Displacement Based Seismic Design of Structures*. IUSS Press, Pavia, Italy.

12 Montejo LA and Kowalsky MJ (2007). *CUMBIA: Set of Codes for the Analysis of Reinforced Concrete Members*. North Carolina State University.

13 Pinto PE (1997). "Seismic design of RC structures for controlled inelastic response". *CEB Bulletin No. 236*.

14 Standards New Zealand (2002). *NZS 1170.0—Part 0: General Principles—New Zealand*. Standards New Zealand, Wellington, NZ.

15 Elwood KJ, Matamoros AB, Wallace JW, Lehman DE, Heintz JA, Mitchell AD and Moore MA (2007). "Update to ASCE/SEI 41 Concrete Provisions". *Earthquake Spectra*, **23**(3): 493–523.

16 ASCE (2017). *Seismic Assessment and Retrofit of Existing Buildings Standard ASCE/SEI 41-17*. American Society of Civil Engineers, USA, 550 pp.

17 Carr A (2016). *Ruaumoko Manual—Volume 5: Appendices, Strength and Stiffness Degradation*. Carr Research Ltd.

18 Dwairi HM, Kowalsky MJ and Nau JM (2007). "Equivalent damping in support of direct displacement-based design". *Journal of Earthquake Engineering*, **11**(4): 512–530. https://doi.org/10.1080/13632460601033884

19 Haselton CB and Deierlein GG (2008). "*Assessing Seismic Collapse Safety of Modern Reinforced Concrete Moment-Frame Buildings*". PEER Report 2007/08, Pacific Earthquake Engineering Research Centre, USA.

20 Fardis MN (2009). *Seismic Design, Assessment and Retrofitting of Concrete Buildings: Based on EN-Eurocode 8*. Springer, 744 pp.

21 Haselton CB, Liel AB, Taylor-Lange SC and Deierlein GG (2016). "Calibration of model to simulate response of reinforced concrete beam-columns to collapse". *ACI Structural Journal*, **113**(6).

22 Tarbali K and Bradley BA (2015). "Ground motion selection for scenario ruptures using the generalised conditional intensity measure (GCIM) method". *Earthquake Engineering and Structural Dynamics*, **44**(10): 1601–1621. https://doi.org/10.1002/eqe.2546

23 Yeow TZ, Orumiyehei A, Sullivan TJ, MacRae GA, Clifton GC and Elwood KJ (2018). "Seismic performance of steel friction connections considering direct-repair costs". *Bulletin of Earthquake Engineering*, **16**(12): 5963–5993. https://doi.org/10.1007/s10518-018-0421-x

24 Galanis PH and Moehle JP (2015). "Development of collapse indicators for risk assessment of older-type reinforced concrete buildings". *Earthquake Spectra*, **31**(4): 1991–2006.

25 Sattar S and Liel AB (2016). "Seismic performance of nonductile reinforced concrete frames with masonry infill walls—II: Collapse assessment". *Earthquake Spectra*, **32**(2): 819–842.

26 Sengupta P and Li B (2016). "Seismic fragility assessment of lightly reinforced concrete structural walls". *Journal of Earthquake Engineering*, **20**(5): 809–840. https://doi.org/10.1080/13632469.2015.1104755

27 Marder K, Motter C, Elwood KJ and Clifton GC (2018). "Testing of 17 identical ductile reinforced concrete beams with various loading protocols and boundary conditions". *Earthquake Spectra*, **34**(3): 1025–1049.

28 Jalayer F and Cornell CA (2009). "Alternative non-linear demand estimation methods for probability-based seismic assessments". *Earthquake Engineering and Structural Dynamics*, **38**(8): 951–972. https://doi.org/10.1002/eqe.876

29 Baker JW (2014). "Efficient analytical fragility function fitting using dynamic structural analysis". *Earthquake Spectra*, **35**: 1077–1095.

30 Matthews J (2004). *Hollow-Core Floor Slab Performance Following a Severe Earthquake*. PhD Dissertation, Department of Civil Engineering, University of Canterbury. https://ir.canterbury.ac.nz/handle/10092/12896

31 MacPherson C (2005). *Seismic Performance and Forensic Analysis of a Precast Concrete Hollow-Core Floor Super-Assemblage*. Master Thesis, University of Canterbury.

32 Corney SR, Ingham JM and Henry RS (2018). "Seismic testing of support connections in deep hollow-core floor units". *ACI Structural Journal*, **115**(3): 735–748.

33 Corney SR, Puranam AY, Elwood KJ, Henry RS and Bull D (2021). "Seismic performance of precast hollow-core floors: Part 1-Experimental data". *ACI Structural Journal*, **118**(5): 49–63.

34 Puranam AY, Corney SR, Elwood KJ, Henry RS and Bull D (2021). "Seismic performance of precast hollow-core floors: Part 2–Assessment of existing buildings". *ACI Structural Journal*, **118**(5).

35 Buker F, Brooke NJ, Elwood KJ, Bull DK, Hogan LS and Parr M (2021). "Development and validation of retrofit techniques for hollow-core floors". *Proceedings of the 2021 Annual SESOC Conference*. Claudelands, Hamilton, NZ.